BIOLOGICAL
CRYSTALLOGRAPHY

Volume 71 (2015)

Supporting information for article:

In meso in situ serial X-ray crystallography of soluble and membrane proteins

Chia-Ying Huang, Vincent Olieric, Pikyee Ma, Ezequiel Panepucci, Kay Diederichs, Meitian Wang and Martin Caffrey

S1. Materials

Monoolein (9.9 MAG) (M239-F4-X) was purchased from Nu-Chek Prep (Elysian, MN) and 7.8 MAG (smm48 and C84) was synthesized and purified in-house, following established procedures (Coleman *et al.*, 2004; Caffrey *et al.*, 2009). Chicken egg white lysozyme (Cat. L6876, lot SLBG8654V), HEPES (Cat. H4034, lot SLBF8768V), sodium acetate (Cat. S2889, lot 079K0122), PEG 400 (Cat. 81172, lot BCBL5307V), sodium bromide (Cat. 71329, lot 132896), hydrochloric acid (Cat. 07102, lot SZBL2500V), ammonium phosphate dibasic (Cat. 09839, lot BCBK1426V) and ammonium phosphate monobasic (Cat. 216003, lot MKBJ9529V) were obtained from Sigma (St. Louis, MO). Sodium chloride (BP358-212, lot 132896) was from Fisher Scientific (Loughborough, U.K.). Microsyringes (Cat. 81030) were sourced from Hamilton (Bonaduz, GR, Switzerland). Cyclic olefin copolymer (COC, Cat. TOPAS 8007) and harvesting cryo-loops (Cat. M2-L18SP-20, M2-L18SP-30 and M2-L18SP-50) were purchased from MiTeGen (Ithaca, NY). Standard glass (127.8 × 85.5 mm^2, 1 mm thick; Cat. 1527127092, lot 29642819) and No. 1.5 glass (124 × 84 mm^2, 0.15 mm thick; Cat. 01029990933, lot 30129819) were obtained from Marienfeld (Lauda-Königshofen, Germany). Perforated double-stick spacer tape (112 × 77 mm^2) of varying thicknesses (50, 64, 140 μm and perforation diameters (6 and 7 mm) (Cat. 9500PC and 9009), and double-stick gasket (2 mm-wide and 140 μm-thick with outer dimensions 118 × 83 mm^2 and inner dimensions 114 × 79 mm^2; TRI-9500PC) were purchased from Saunders (St. Paul, MN). Glass cutters (TCT Scriber & Glass Cutter, Cat. 633657) were obtained from Silverline (Yeovil, UK). Rain-X rain repellent (Cat. 80199200, lot 5026349013414) was from Shell Car Care (*Altrincham*, *Cheshire*, U.K.).

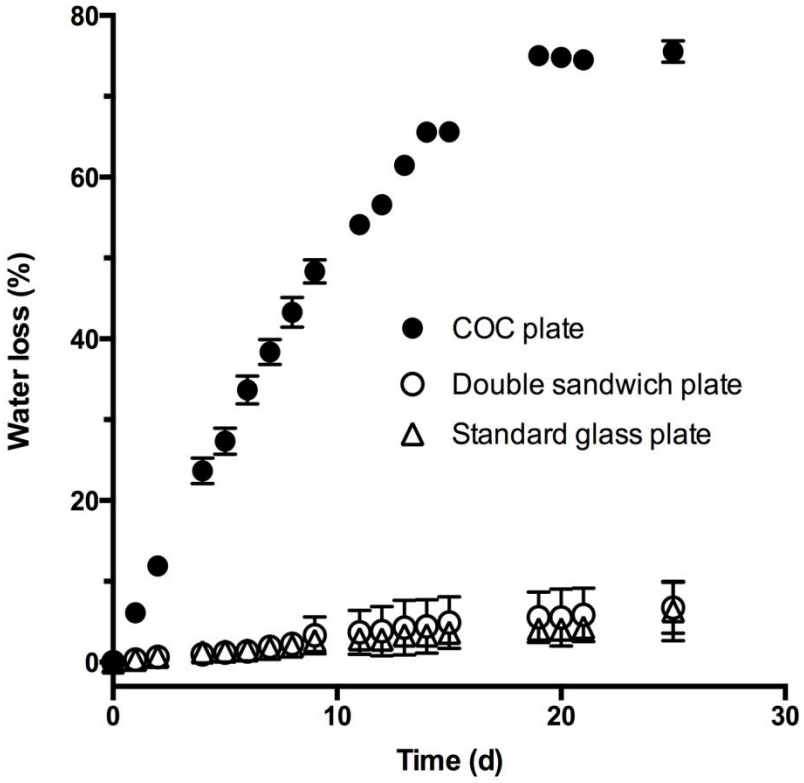

Figure S1 Time-dependent loss of water from COC sandwich plates, double sandwich IMISX plates and standard glass sandwich plates at 20 °C. Measurements were made with 96-well plates stored in a temperature-regulated incubator with 800 nL precipitant solution in each well as described under Methods. The total mass of precipitant on a plate as a function of time was recorded over a period of 25 days. Precipitant mass at time zero was approximately 70 mg.

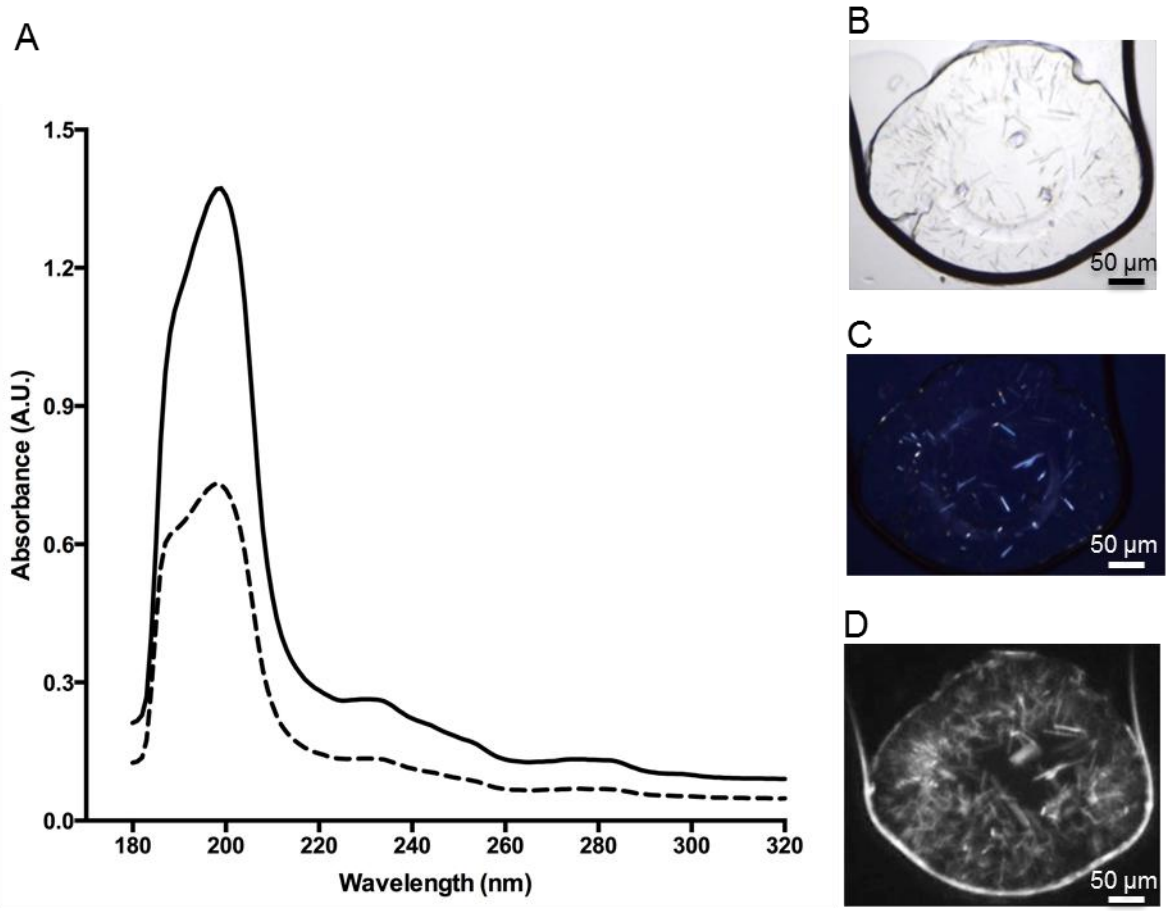

Figure S2 Spectral absorbance, transmission and transparency properties of COC film and plates used for IMISX measurements. (*A*) Absorption spectrum of one (dashed line) and two pieces (solid line) of COC film, 25 µm-thick, as used in IMISX plates. Spectra were recorded against air. Images of membrane protein crystals growing in the cubic phase housed in COC sandwich plates recorded by bright field (*B*) and cross polarized light microscopy (*C*) and by UV fluorescence microscopy (*D*). Images were recorded using a Rockimager 1000 (Formulatrix) that included an ultraviolet imaging device.

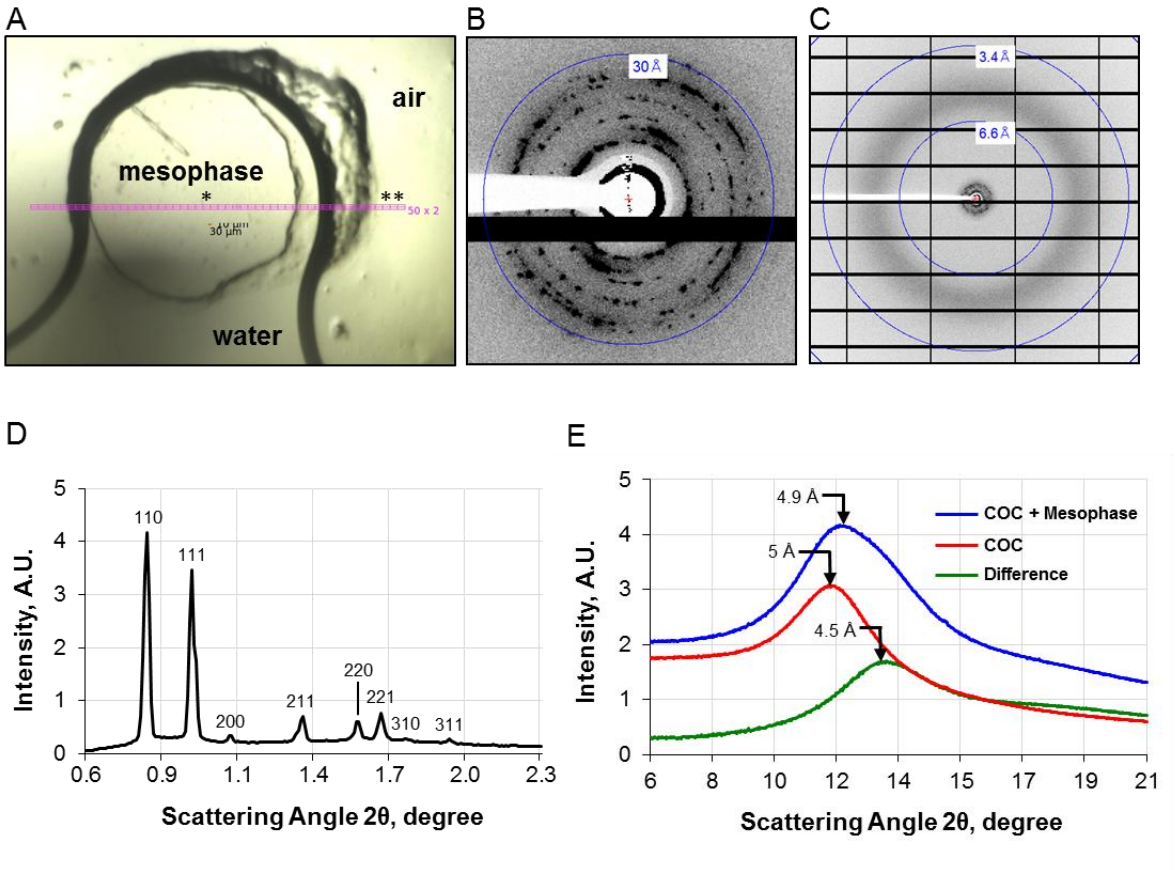

Figure S3 SAXS and WAXS from the cubic-Pn3m phase of fully hydrated 9.9 MAG in an IMISX well at room temperature. (*A*) IMISX sample used for SAXS/WAXS reference measurements mounted on a goniometer at beamline PXII (X10SA) viewed through the COC window with an on-axis microscope. The horizontal two-row grid identifies the section of the sample used for SAXS measurements made with a 30 × 10 μm^2 beam in sequential horizontal steps of 30 μm and an exposure time of 0.1 s at a sample-to-detector distance of 490 mm and a wavelength of 1.0331 Å. The sample was prepared by incubating a 200 nL bolus of molten 9.9 MAG in 1 μL Milli-Q water sealed in an IMISX well for 3 hours at room temperature. Sample thickness was 190 μm which included the 50 μm of COC film and 140 μm of mesophase. (*B*) SAXS pattern recorded in the grid sector marked with an asterisk in (*A*). The resolution marker (circular dashed line) corresponds to 30 Å. The spotty SAXS pattern derives from microdomains of which the liquid crystalline sample is constituted. (*C*) WAXS and SAXS pattern recorded as in (*B*) with resolution markers at 6.6 and 3.4 Å. (*D*) Circular averaging of the SAXS pattern in (*B*) with data presented in the form of an intensity versus *d*-spacing and scattering angle (I/2θ) plot. Low-angle powder peaks, identified by Miller indices (*hkl*), index in the cubic-*P*n3m space group with *d*-spacing values of 71.2 Å (*110*), 58.63 Å (*111*), 50.93 Å (*200*), 41.05 Å (*211*), 35.79 Å (*220*), 33.88 Å (*221*), 32.16 Å (*310*) and 29.45 Å (*311*) and relative *d*-spacing values of 1.00, 1.21, 1.40, 1.73, 1.99, 2.10, 2.21 and 2.42, respectively. For a cubic space group, the unit cell parameter, *a*, equals $d(h^2 + k^2 + l^2)^{1/2}$. A line of best fit to data plotted as *d* versus ($h^2 + k^2 +$

$l^2)^{-1/2}$ for the 8 peaks has a slope a = 101.3 Å (r^2 = 0.9997). A similar value has been reported for fully hydrated 9.9 MAG in sealed glass X-ray capillaries at 20 °C (Caffrey, 1987). The black ring to the center of the pattern is due to X-ray scattering from and leakage around the beamstop. (*E*) Circular averaging of the WAXS region of the pattern in (*C*) with data presented as in (*D*). Patterns were recorded in the sample at grid sectors marked by single and double asterisks in (*A*) corresponding to mesophase plus COC windows (blue line) and to COC windows alone (red line), respectively. A difference I/2θ profile corresponding to scattering from the mesophase alone is included (green line). COC has a diffuse scattering peak centered at ~5.0 Å. Scattering from 'molten' chains in the mesophase is also broad, with a maximum at ~4.5 Å, as observed previously (Caffrey, 1987).

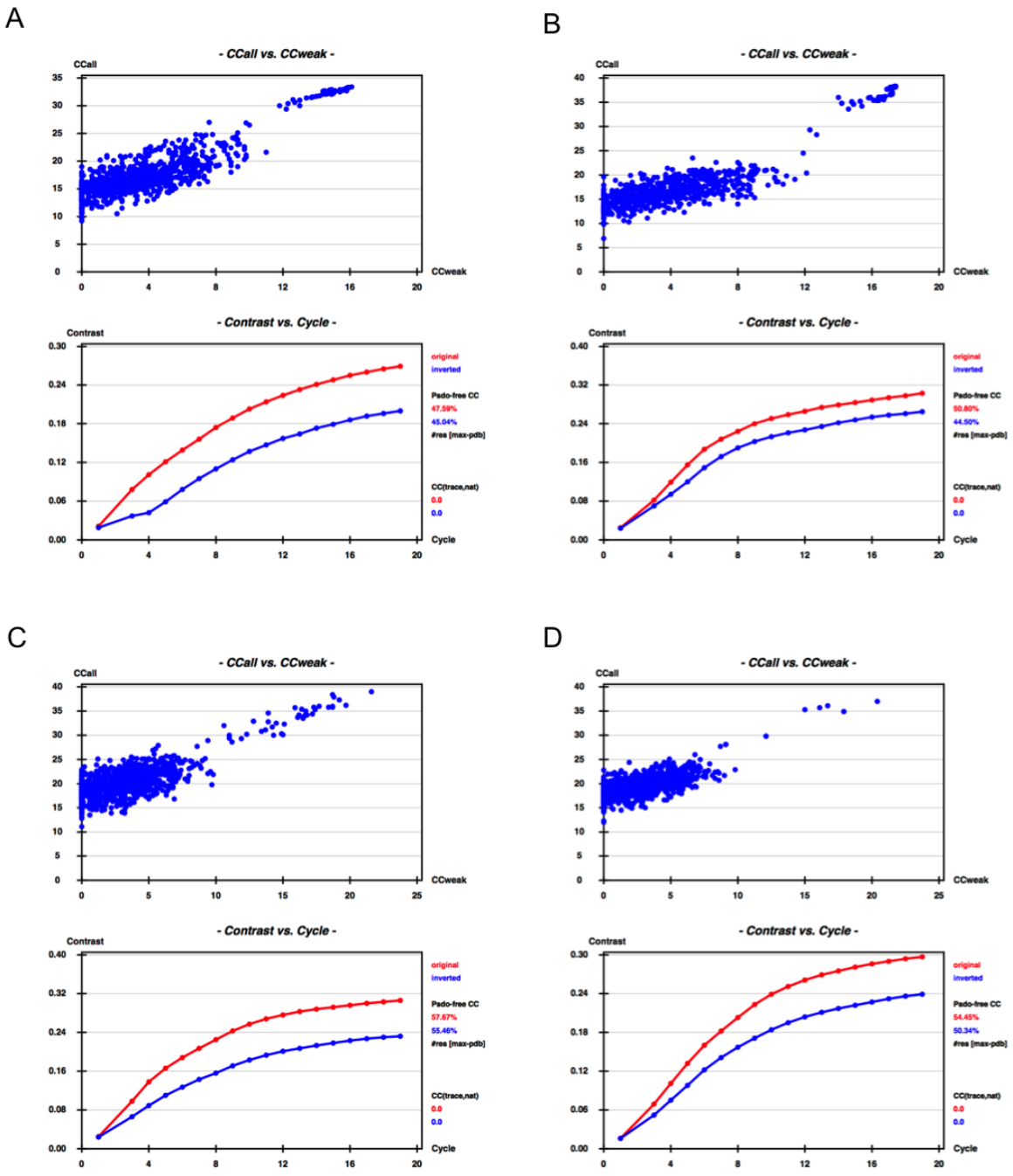

Figure S4 Substructure and hand determination with SHELXD/E. (*A*) Lysozyme Br-SAD IMISX data. (*B*) Lysozyme Br-SAD 100 K data. (*C*) Lysozyme S-SAD IMISX data. (*D*) Lysozyme S-SAD 100 K data.

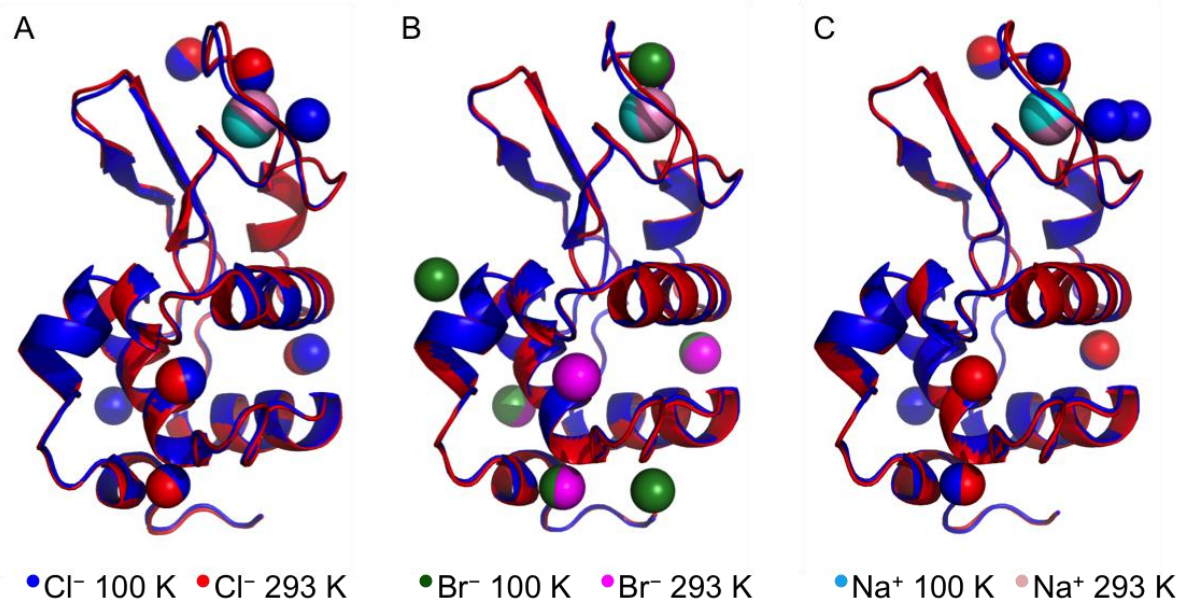

Figure S5 Structure of lysozyme solved by molecular replacement (*A*), Br-SAD (*B*) and S-SAD phasing (*C*) using *in situ* crystals at room temperature (red ribbon model) and harvested crystals at 100 K (blue ribbon model). Structured ions are shown as spheres coloured as follows: chloride, blue (100 K) and red (293 K); bromide, green (100 K) and magenta (293 K); sodium, light blue (100 K) and pink (293 K). The r.m.s.d. over 129 residues for backbone atom positions between 100 K and 293 K models obtained by molecular replacement, Br-SAD and S-SAD phasing were 0.257 Å, 0.169 Å and 0.196 Å, respectively.

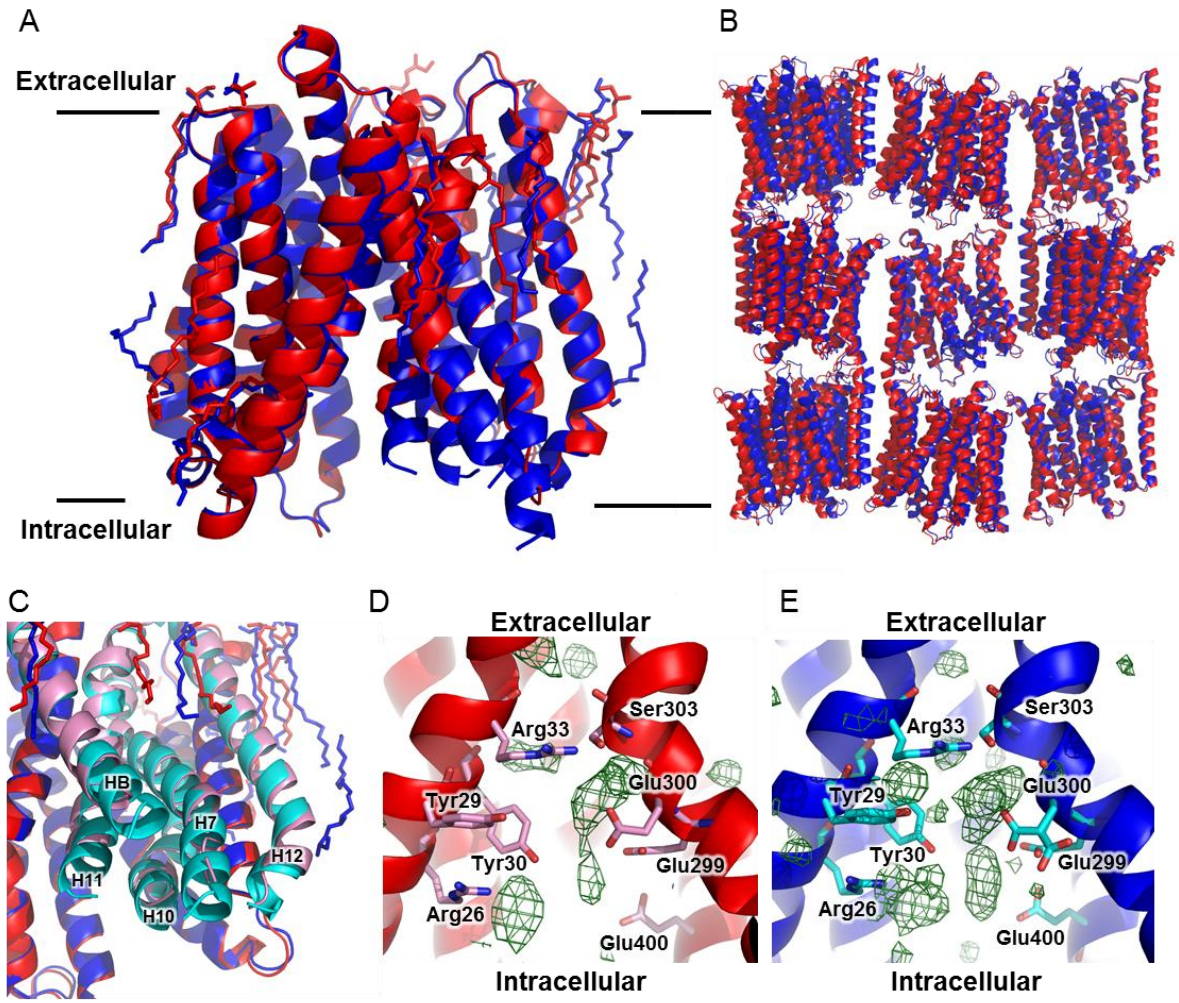

Figure S6 A comparison of the structures of $PepT_{St}$ obtained using IMISX at room temperature and by conventional cryo-crystallography at 100 K. (*A*) Superposition of $PepT_{St}$ structures at room temperature (red) and at 100 K (blue). The view is from within the membrane, the approximate limits of which are marked by horizontal black lines. Lipid and detergent molecules are in stick representation. (*B*) The packing arrangement in crystals of $PepT_{St}$. Room temperature and 100 K structures are shown superposed with color coding as in (*A*). The layered or Type I packing is typical of *in meso* grown crystals. (*C*) An expanded view of parts of the $PepT_{St}$ that differ in structure between that recorded at room temperature and at 100 K. Sections of the protein that show differences are colored pink and light blue corresponding to structures at room temperature and 100 K, respectively. Helix (H) identities are as described in the text. A view into the 'peptide' binding pocket of $PepT_{St}$ at room temperature (*D*) and at 100 K (*E*) revealing unaccounted for electron density (green mesh; Fo−Fc omit density maps contoured at 3 σ) referred to in the text. Conserved residues proposed to partake in peptide binding and transport are identified and shown in stick representation.

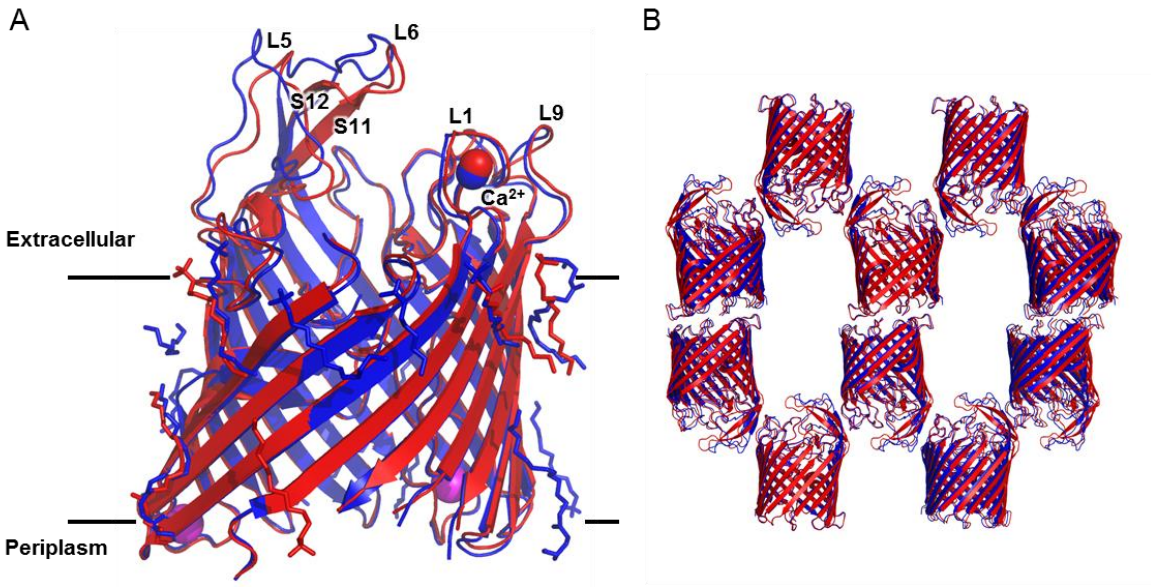

Figure S7 A comparison of the structures of AlgE obtained using IMISX at room temperature and by conventional cryo-crystallography at 100 K. (*A*) Superposition of AlgE structures at room temperature (red) and at 100 K (blue). The view is from within the membrane, the approximate limits of which are marked by horizontal black lines. Lipid and detergent molecules are shown as stick figures and calcium as spheres. Copper has been reported to occupy the calcium site in L1. An X-ray fluorescence scan performed on an AlgE crystal in an IMISX well at room temperature showed no evidence for copper. The density was best explained by calcium. Extracellular loops (L1, L5, L6, L9) and β-strand (S11 and S12) that differ between the two data set types and/or that are involved in crystal contacts are labelled. The two sodium cations were colored magenta which only showed in room temperature structure. (*B*) The packing arrangement in crystals of AlgE. Room temperature and 100 K structures are shown superposed with color coding as in (*A*). Crystal contacts on the extracellular side of AlgE involve loops L5 and L6 and β-strand S11 and S12 of one molecule and L1 and L9 of another.

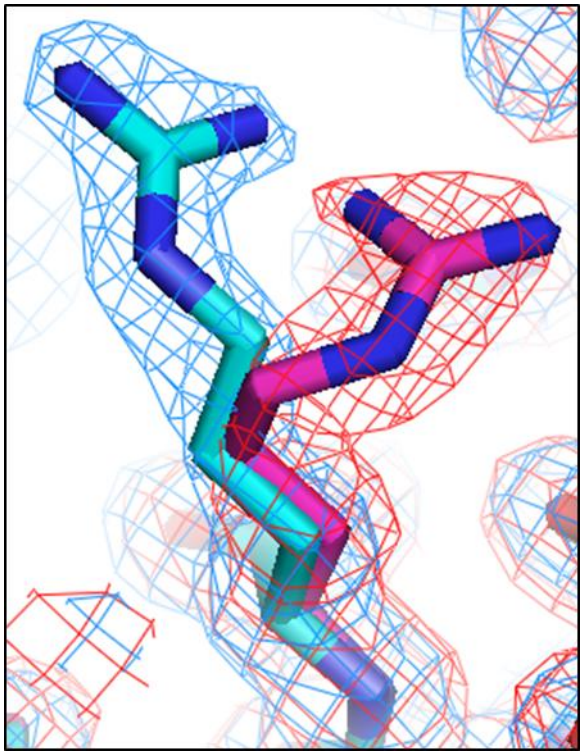

Figure S8 Alternative conformations observed for the side chain of Arg112 in native lysozyme crystals at room temperature (magenta) and at 100 K (light blue). Electron density maps are shown as red and light blue meshes contoured at 1 σ. Stick representation is shown (carbon, red and light blue; nitrogen, blue). Arg112 is located on the surface of lysozyme to the periphery of the substrate binding cleft.

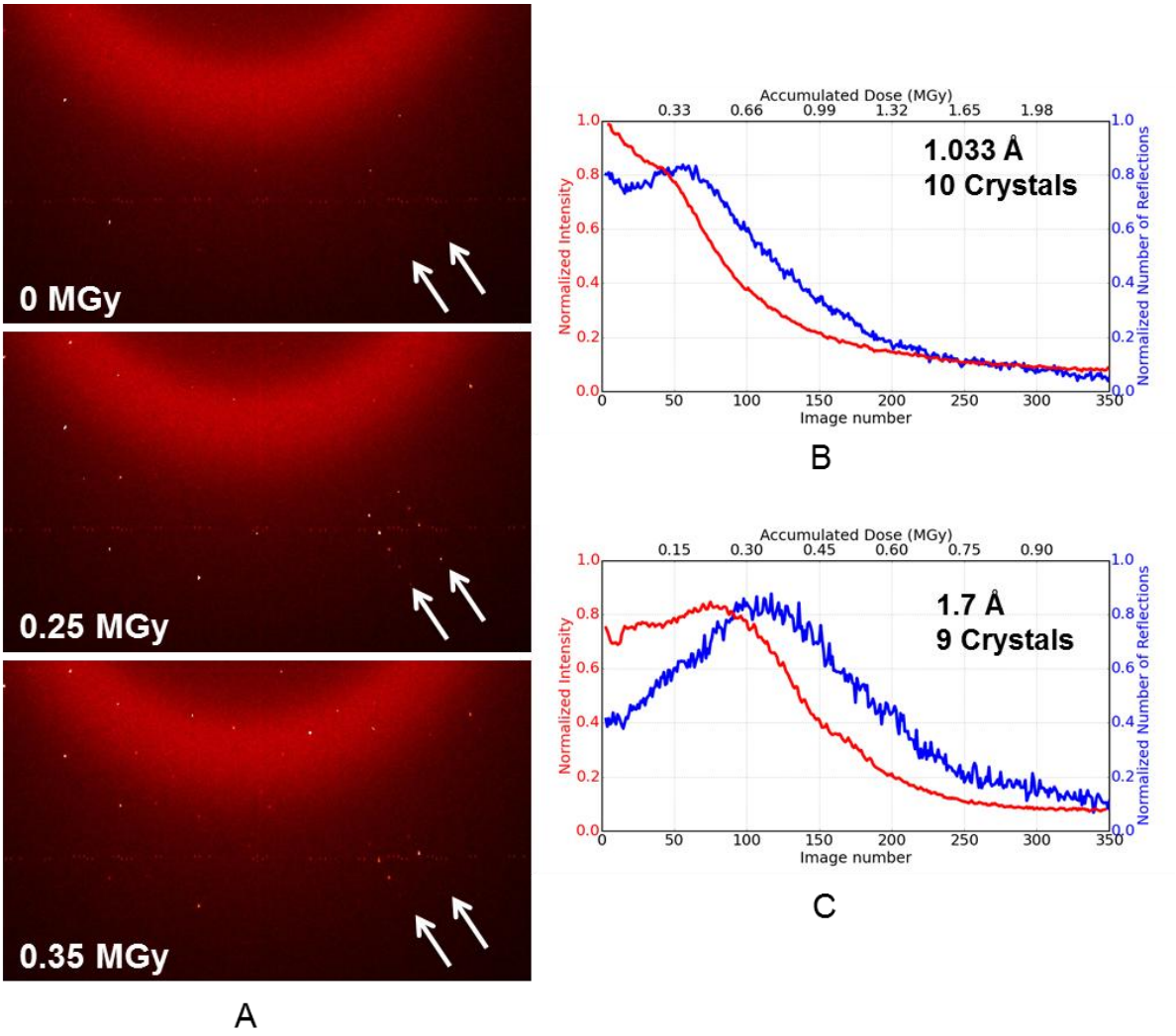

Figure S9 The effect of accumulated X-ray dose on diffraction characteristics of native lysozyme crystals in IMISX plates at room temperature. Crystals were stationary and were not rotated during the course of the exposure. (*A*) Diffraction at wide angles recorded from a single, fixed crystal at increasing accumulated dose at 1.7 Å. Images shown are the sum of five sequential frames. The arrows point in directions where the coming and going of reflections due to radiation damage is particularly apparent. Diffuse scatter from the COC windows and the mesophase reaches a maximum at around 4.9 Å. (*B*, *C*) Normalized and averaged total crystal diffraction intensity and normalized number of reflections per image as a function of image number and accumulated dose. The total number and intensity of all reflections on each still image was calculated using custom spot finding and integration Python scripts. Total intensities were summed, normalized and averaged over all crystals (10 crystals at 1.033 Å, 9 crystals at 1.7 Å). There is a peak in number of reflections early in the exposure. This transient rise is attributed mainly to reciprocal lattice points that move into the Ewald sphere and into diffraction condition by the damage-induced increase in mosaicity. A 357-frame movie of diffraction images of the type represented in Fig. S9C? is included under Supplementary Movie.

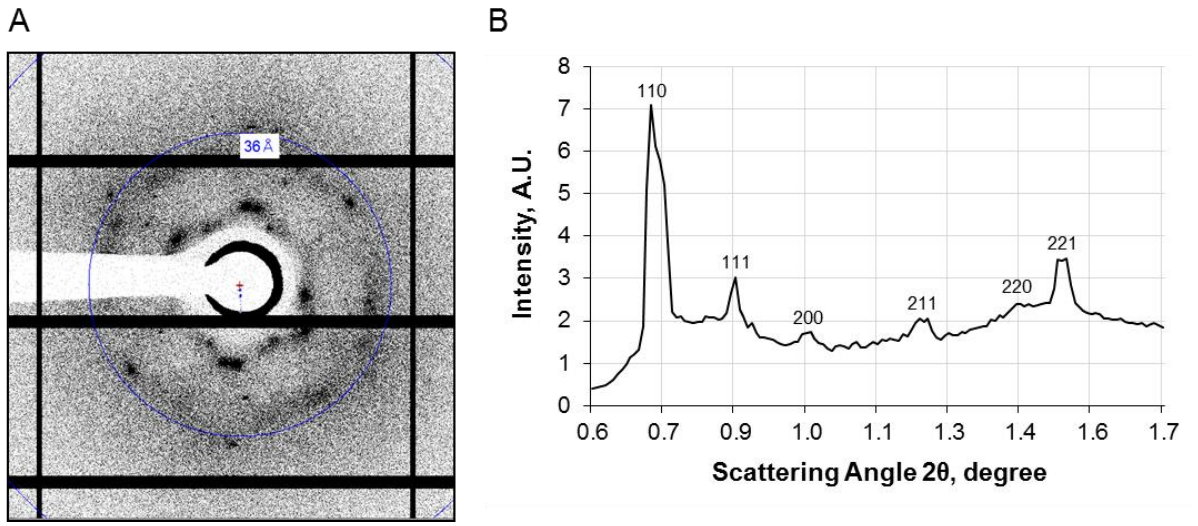

Figure S10SAXS from the cubic-Pn3m phase of fully hydrated 7.8 MAG in an IMISX well at room temperature. (*A*) SAXS pattern recorded as described in **Supplementary Fig. S3**. The resolution marker (blue circle) corresponds to 36 Å. (*B*) Circular averaging of the SAXS pattern in (*a*) with data presented as an I/2θ plot, as in **Supplementary Fig. S3**. Low-angle powder peaks, identified by Miller indices, index in the cubic-*P*n3m space group with *d*-spacing values of 83.06 Å (*110*), 67.09 Å (*111*), 58.15 Å (*200*), 47.47 Å (*211*), 40.57 Å (*220*) and 38.34 Å (*221*) and relative *d*-spacing values of 1.00, 1.24, 1.43, 1.75, 2.05 and 2.17, respectively. The corresponding unit cell parameter, *a*, calculated as in the legend to **Supplementary Fig. S3**, is 115.5 Å (r^2 = 0.9992). The black ring to the center of the pattern is due to X-ray scattering from and leakage around the beamstop.

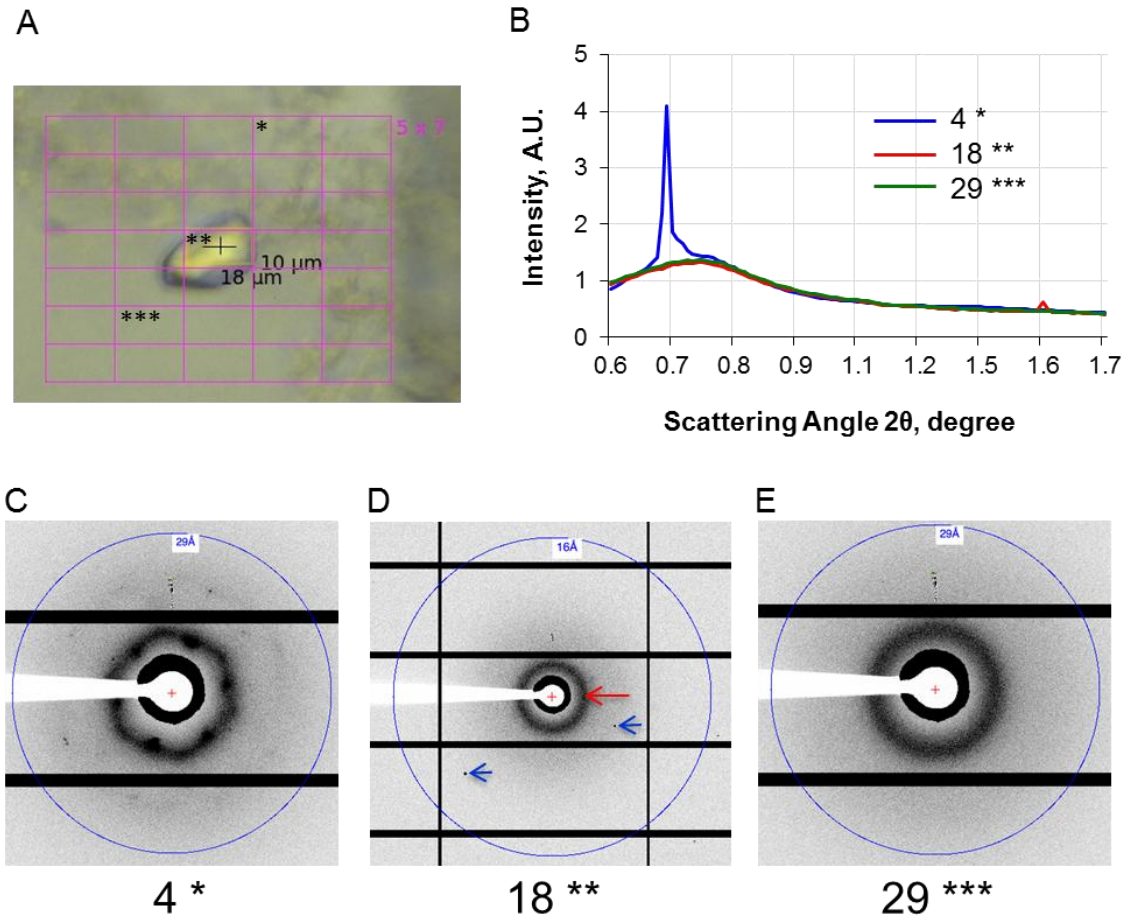

Figure S11 SAXS characterization of the mesophase in the vicinity of a $PepT_{St}$ crystal in an IMISX well at room temperature with 7.8 MAG as the host lipid. The precipitant included 250–325 mM $NH_4H_2PO_4$, 100 mM HEPES, pH 7.0 and 21–22 %(*v*/*v*) PEG 400. (*A*) View of a crystal growing in the mesophase, with a rastering grid superimposed, in preparation for SAXS measurements. The beam and raster sector sizes are 18 × 10 µm^2. I/2θ plot (*B*) of the SAXS data recorded on sample in (*A*) at grid sectors 4 (blue line) (*C*), 18 (red line) (*D*) and 29 (green line) (*E*), as in **Supplementary Fig. S3**. The diffuse low-angle band, with a scattering maximum at ~75 Å, derives from the sponge phase (red arrow in (*D*). The sharp reflections derive from the $PepT_{St}$ crystals (blue arrows in *D*). The diffuse scatter and sharp peaks in the profile recorded in sector 4 indicate that the sponge and cubic phases coexist at this location in the sample. Assuming the latter is of the cubic-*Pn3m* type, it indexes with a unit cell length of 115.9 Å (see legend, **Supplementary Fig. S3**). At locations in the sample corresponding to sectors 18 and 29, the sponge phase alone is present.

Table S1 Facts and figures used to estimate the accumulated dose per crystal for the IMISX data recorded and the radiation damage study performed at 293 K

Experiment	IMISX					Radiation damage study	
Protein	Lyso-Native	Lyso-Br	Lyso-S	$PepT_{St}$**	AlgE	Lyso-Native	Lyso-S
Crystal size (μm^3)	10×10×20	10×20×30	10×10×20	10×10×20	5×5×20	20×20×40	20×20×40
Wavelength (Å)	1.0332	0.9205	1.7000	1.0332	1.0332	1.0332	1.7000
Energy (keV)	12.000	13.469	7.293	12.000	12.000	12.000	7.293
Flux (photons/s)	3×10^{11}	1.5×10^{10}	9×10^{9}	3×10^{11} 7.5×10^{10}	1.5×10^{11}	3×10^{12}	5×10^{11}
Beam size (μm^2)	10 × 18	10 × 18	10 × 30	10 × 18	10 × 10	10 × 50	10 × 50
Estimated dose rate (MGy/s)*	0.889	0.083	0.042	0.889 0.222	0.800	3.202	1.445
Oscillation / exposure (° / s)	0.2 / 0.05	0.1 / 0.1	0.1 / 0.1	0.2 / 0.05 0.1 / 0.1	0.2 / 0.05	0	0
Oscillation range/crystal (°)	1.2	2	2	0.6	1	0	0
Exposure time/ crystal (s)	0.3	2.0	2.0	0.15 0.6	0.25	1	1
Estimated accumulated dose/crystal (MGy)*	0.267	0.166	0.084	0.133 0.133	0.200	3.3	1.5
Total number of crystals	113	239	992	237 335	175	–	–
Total degree/ data set (°)	113	478	1984	142.2 201	175	–	–
Total exposure time/data set (s)	33.9	478	1,984	236.6	43.8	–	–
Total dose/data set (MGy)	30	39	83	76	35	–	–

* estimate based on Equation 1 in Holton (Holton, 2009). For Lyso-Br crystals at the Br K-edge, the 'dose-doubling' effect of an estimated 0.38 M bromide in the crystal, assuming a solvent content of 38%, has been accounted for. Solvent content was calculated based on a combined lysozyme + 51 structured waters molecular weight of 15,191 Da and the Matthews Probability Calculator (http://www.ruppweb.org/mattprob/default.html)

** two different flux and oscillation/exposure values used

Table S2 Sample consumption and diffraction measurement statistics

Supplementary Table S2

Temperature /Presentation	100 K / Loop					293 K / *In situ*				
Protein	Lyso-Native	Lyso-Br	Lyso-S	$PepT_{St}$	AlgE	Lyso-Native	Lyso-Br	Lyso-S	$PepT_{St}$	AlgE
MAG	9.9	9.9	9.9	7.8	7.8	9.9	9.9	9.9	7.8	7.8
Mesophase/well (nL)	200	200	200	66	50	200	200	200	66	50
Lipid/protein soln (by vol.)	3/2	3/2	3/2	1/1	1/1	3/2	3/2	3/2	1/1	1/1
Protein conc. (mg/mL)	50	50	50	10	10	50	50	50	10	10
No. wells	1	1	1	1	1	2	4	12	20	1
No. crystals	1	1	3	1	1	114	279	1,290	1,363	484
No. useful crystals	1	1	3	1	1	113	239	992	572	175
Index rate (%)	100	100	100	100	100	99.1	85.6	76.8	41.9	36.2
Lipid (μL)	0.12	0.12	0.12	0.033	0.025	0.24	0.48	1.44	0.66	0.025
Protein (μg)	4	4	4	0.33	0.25	8	16	48	6.6	0.25
Total degrees / crystal	100	720	360	120	140	2	2	2	1, 2*	3
Useful degrees / crystal	100	720	360	120	140	1.2	2	2	0.6	1
Oscillation (^{o} / frame)	0.1	0.1	0.1	0.1	0.5	0.2	0.1	0.1	0.1, 0.2*	0.2
Degrees (^{o}), total	100	720	1,080	120	140	135.6	478	1,984	343.2	175

***** Some crystals were measured with 0.1 ^{o} /frame, others were measured with 0.2 ^{o} /frame.

Table S3 Differences in lysozyme, $PepT_{St}$ and AlgE structures determined by the IMISX method at room temperature and by conventional crystallography in loops at 100 K.

(*a*) Lysozyme

Residue	**Differences, RT *vs*. 100 K**		
	Lyso-Native	**Lyso-Br**	**Lyso-S**
R14	*	**	*
L17	*	*	*
D18	***	**	**
N19	**	**	*
R21	*	*	*
R45	*	*	*
N46	*	-	-
T47	*	-	*
D48	*	-	-
I55	*	-	-
N59	*	**	-
R61	*	*	***
P70	*	-	-
R73	**	**	**
N77	***	***	**
S86	-	***	-
D87	**	*	-
D93	**	-	-
K97	*	**	****
D101	***	*	-
D103	*	*	*
V109	*	*	*
A110	*	-	-
R112	**	**	***
N113	*	*	-
D119	*	*	*
Q121	****	*	**
R125	*	*	**
R128	*	***	*
L129	*	**	*

- very similar to identical

* slightly different

** different conformers

*** multiple side chain conformers in the RT structure

**** poor electron density at this residue

(*b*) $PepT_{St}$.

Residue /Segment[a]	**Features**			**Differences**[d]
	RT[b]	**100 K**[b]	**100 K**[c] **PDB 4D2B**	
E300	Conf. A	Conf. A, B	Conf. A, B	***
N-ter.	G5-P12 (M1-K4)	G5-P12 (M1-K4)	K6-P12 (M1-G5)	*
H1	L13-T46	L13-T46	L13-T46	-
H2	R53-I81	R53-I82	T52-I81	-
H3	A84-A103	A84-A103	G83-L104	-
H4	A108-L136	A108-L136	G107-L136	*
H5	R142-A173	R143-A173	R143-A172	*
H6	Y175-T200	Y175-T200	G174-T200	-
HA	P214-V241	P214-V241	A213-V241	*
HB	L246-F265 (W267-H279)	L246-S270 (V272-V274)	S245-S270 (S271-H279)	**
H7	S284-E312	T277-E312	R281-V314	**
H8	V321-A345	V321-A345	P320-W343 (L346-A348)	*
H9	S353-Y378	S353-Y378	S352-G379	*
H10	P386-S409 (T411-M423)	P386-K413 (A415-F419)	P386-T412 (K413-Q422)	**
H11	S425-L444	S421-L444	M423-Y445	**
H12	S449-I475 (Q476-E483)	S449-G477 (M479-E483)	S449-L471 (K473-E483)	**

[a] notation as in Lyons *et al*., 2014

[b] this work. Missing residues are shown in closed brackets.

[c] this $PepT_{St}$-apo structure, from Lyons *et al*. (Lyons *et al*., 2014), is included as a reference. Missing residues are shown in closed brackets.

[d] comparing RT and 100 K structures reported in this work with the following structure difference ratings:

- little or no difference

* same secondary structure, but slightly misaligned

** residues missing and secondary structure changed

*** conformer differences. See Supplementary Fig. S6*D*, *E*.

(*c*) AlgE.

Residue /Segment[a]	**Features**			**Differences**[d]
	RT[b]	**100 K**[b]	**100 K**[c] **PDB 4AFK**	
N-ter.	P39-N41	P39-N41	E37-N41	-
S1	F42-E53	F42-N54	F42-N54	-
L1	N54-T65	D55-T65	D55-T65	***
S2	L66-Q80	L66-Q80	L66-W81	-
T1	W81--D83	W81--D83	G82-D83	-
S3	W84-A94	W84-A94	W84-A95	-
L2	A95-K123 (D107-P121)	A95-K123 (D109-P120)	T96-K123 (D109-N116)	**
S4	S124-D134	S124-D134	S124-Y135	-
T2	Y135- G143	Y135- G143	A136-G143	-
S5	E144- L153	E144-L153	E144-R154	-
L3	R154- Q161	R154-Q161	E160-Q161	-
S6	D162- P172	D162-P172	D162-E173	-
T3	E173-L176	E173-L176	T174-L176	*
S7	L177-A184	L177-A184	L177-Q185	-
L4	Q185-D203	Q185-D203	R186-D204	*
S8	R205-W215	R205-W215	R205-A216	-
T4	A216-H218	A216-H218	P217-H218	-
S9	H219-D229	H219-D229	H219-D230	*
L5	D230-G250	D230-G250	S231-T247	***
S10	Q251-T260	Q251-T260	Y248-G261	-
T5	G261-P271	G261-P271	D262-P271	-
S11	L272-T291	L272-N287	L272-T292	***
L6	V292-R297	L288-G301	V293-R296	***
S12	I298-W318	K302-W318	R297-N319	***
T6	N319-Q323	N319-Q323	I320-Q323	-
S13	W324-R332	W324-R332	W324-G333	-
L7	G333-S375	G333-N376	S334-N376	*
S14	N376-Q387	L377-Q387	L377-L388	-
T7	L388-E390	L388-E390	R389-D391	*
S15	D391-W402	D391-W402	Y392-R403	-
L8	R403-D425	R403-D425	V404-K424	*
S16	I426-K435	I426-K435	D425-Y437	-
T8	Y437-L457 (Q440-P454)	Y437-L457 (K439-P454)	F438-A456 (K439-P454)	**
S17	I458-K466	I458-K466	L457-P467	-
L9	P467-T478	P467-T478	G468-T478	***
S18	M479-W488	M479- R489	M479-R489	-
C-ter.	R489- F490	F490	F490	**

[d] comparing RT and 100 K structures reported in this work with the following structure difference ratings and notes:

- identical

* same secondary structure, but slightly misaligned align

** residues missing and secondary structure changed

*** involved in crystal contact

References

Caffrey, M. (1987). *Biochemistry* **26**, 6349-6363.

Caffrey, M., Lyons, J., Smyth, T. & Hart, D. J. (2009). *Curr. Top. Membr.* **63**. *83–108.*

Coleman, B. E., Cwynar, V., Hart, D. J., Havas, F., Mohan, J. M., Patterson, S., Ridenour, S., Schmidt, M., Smith, E. & Wells, A. J. (2004). *Synlett* **8**, 1339–1342.

Holton, J. M. (2009). *J. Synchrotron Radiat.* **16**, 133-142.

Lyons, J. A., Parker, J. L., Solcan, N., Brinth, A., Li, D., Shah, S. T., Caffrey, M. & Newstead, S. (2014). *EMBO rep.* **15**, 886-893.

Tan, J., Rouse, S. L., Li, D., Pye, V. E., Vogeley, L., Brinth, A. R., El Arnaout, T., Whitney, J. C., Howell, P. L., Sansom, M. S. & Caffrey, M. (2014). *Acta Cryst.* D**70**, 2054-2068.

Supplementary Movie

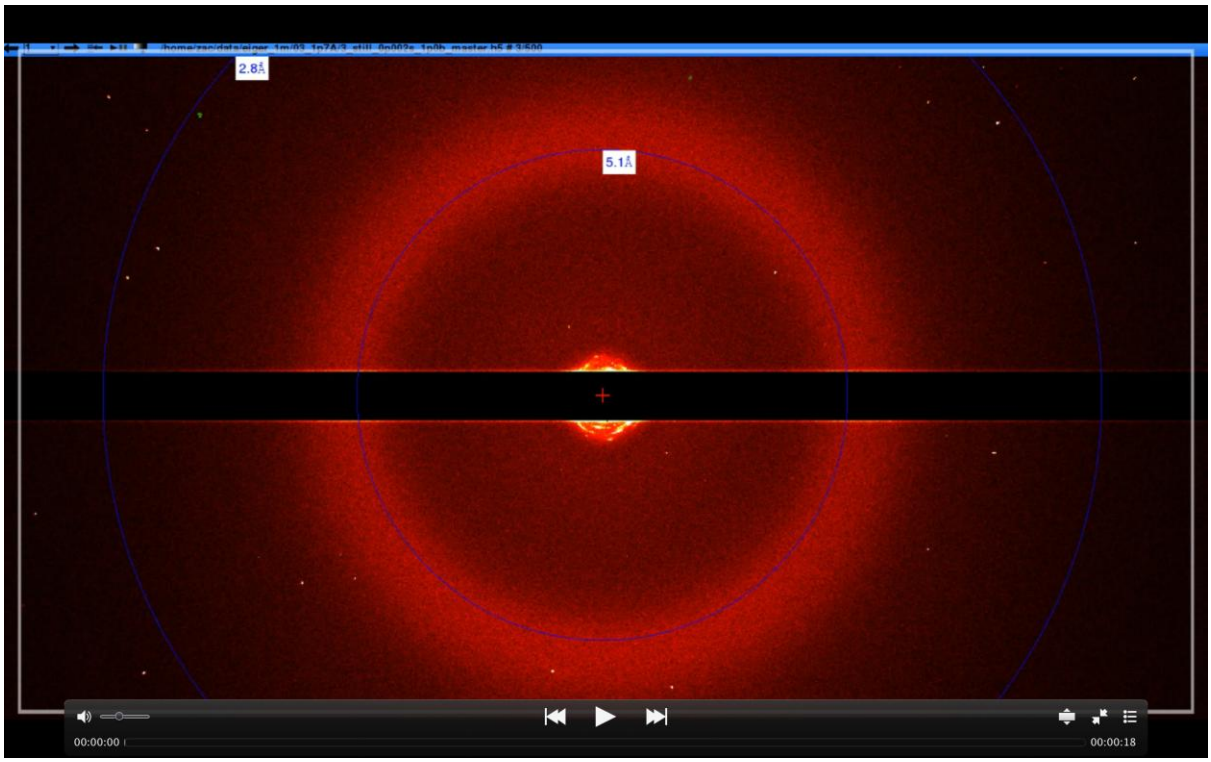

Still Image and Legend for Movie

Supplementary Movie S1. The effect of accumulated X-ray dose on diffraction characteristics of native lysozyme crystals in IMISX plates recorded at room temperature with the EIGER 1M detector operating at 500 images/second and a readout time of 20 μs. Crystals were stationary and were not rotated during the course of the exposure with a 10 × 50 μm^2 sized unattenuated beam at 1.7 Å. Diffuse scatter from the COC windows and the mesophase reaches a maximum at around 4.9 Å. See Fig. S9.